Netherlands Journal of Geosciences — Geologie en Mijnbouw |95 – 1 | 3–22 | 2016 doi:10.1017/njg.2015.25

Thin section petrography and chemostratigraphy: Integrated evaluation of an upper Mississippian mudstone dominated succession from the southern Netherlands

C.J. Nyhuis[1,*], D. Riley[2] & A. Kalasinska[3]

1 Institut für Geologie und Mineralogie, Universität zu Köln, Zülpicher Str. 49A, D-50674 Köln, Germany
2 Chemostrat Ltd, Ravenscroft Court, Buttington Cross Enterprise Park, Welshpool, Powys SY21 8SL, UK
3 Origin Analytical Ltd, Ravenscroft Court, Buttington Cross Enterprise Park, Welshpool, Powys, SY21 8SL, UK
* Corresponding author. Email: chr.nyhuis@gmail.com

Manuscript received: 01 October 2014, accepted: 09 August 2015

Abstract

Sedimentological data acquired by thin section petrography is a rich source of information to better understand and interpret depositional environments that are dominated by fine-grained deposits. This study provides an evaluation of the sedimentological and geochemical changes recorded over Upper Viséan to Lower Namurian successions preserved in a core section from a well drilled in the southern part of the Netherlands. Facies analysis and the recognition of microfacies associations allow detailed interpretations of depositional environments. Interpretation of additional geochemical data acquired by portable X-ray fluorescence analyses has resulted in a chemostratigraphic zonation for the core section. The zonation reflects stratigraphic changes in the mineralogy of the sedimentary successions. Integration of the microfacies associations and the chemostratigraphic zonation has led to the identification of three so-called depositional zones, which show the development of depositional settings from Late Viséan to Early Namurian times. Depositional Zone 1 consists of fine-grained turbiditic limestones and mudstones deposited in a distal carbonate ramp setting during Latest Viséan times. The overlying Depositional Zone 2 corresponds to the Geverik Member (Lower Namurian) and is particularly heterogeneous in geochemical and lithological terms: the zone reflects a complex interplay between different parameters such as sediment source, transport mechanisms and oxygen content that are assumed to be governed by fluctuating sea levels and changing depositional environments (from basinal to shallow marine settings). Sandy lenticular mudstones are predominant in the lower part of Depositional Zone 2 and show that sedimentation was via erosive bedload, whilst the common fossiliferous mudstones present within the upper part of the same zone yield evidence for increased endobenthic activity in dysoxic conditions. The successions assigned to Depositional Zone 3 (= Epen Formation – Namurian) are the products of cyclic sedimentation of a terrestrial sourced delta.

Keywords: black shale, Carboniferous, depositional environment, drill core, portable XRF

Introduction

Increasing interest is now focused on Carboniferous black shales in northwest Europe due to recent advances in unconventional shale-gas exploration. Published information about these rocks relates to their hydrocarbon potential, characterisation and possible potential for shale-gas exploration (Gerling et al., 1999; Hartwig et al., 2010; Littke et al., 2011; Van Bergen, 2011; Uffmann et al., 2012; Kerschke & Schulz, 2013). However, only a few published works on these black shales have incorporated data derived from thin section petrography (e.g. Davies et al. (2012), Könitzer et al. (2014) and Nyhuis et al. (2014)). Thin section petrography is regarded by the current authors as an important method for acquiring significant information about the mineralogy and texture of the fine-grained rocks. Such information is indispensable for modelling depositional environments and provides reliable insight into transport mechanisms, fossil content and degree of bioturbation.

Previous studies on many Palaeozoic and Mesozoic black shale successions have revealed that they reflect a complex interplay of different mudstone types and a very heterogeneous microfacies association despite their macroscopic homogeneity

(Schieber, 1999; Loucks & Ruppel, 2007; Lemiski et al., 2011; Trabucho-Alexandre et al., 2012; Abouelresh & Slatt, 2012), highlighting the importance of detailed rock descriptions and microfacies analysis in relation to unconventional shale-gas exploration. To avoid misinterpretations of the depositional environments relating to these successions, the current authors recommend establishing a microfacies framework for the shales prior to any further investigations, such as geochemical analysis.

The whole-rock geochemistry of the black shale successions reflects their mineral assemblages, which in turn have been influenced by provenance and depositional environments, weathering processes during transport and deposition, burial diagenesis and changing temperature/pressure regimes. Geochemical datasets can be acquired through inductively coupled plasma (ICP) spectrometry. Chemostratigraphy employs such datasets to establish chemostratigraphic zonations and correlations. The various divisions of the zonations reflect stratigraphic variations in the geochemical composition of the strata (Pearce et al., 2005; Ratcliffe et al., 2010, 2012a, b; Ratcliffe & Wright, 2012). Although heavy atoms fluoresce, which may cause interelemental interferences and hinder quantitative evaluations, advances in the utilisation of X-ray fluorescence (XRF), such as the development of unique certified reference materials (CRMs), has led to its use in chemostratigraphy (Rowe et al. 2009, 2012). Portable XRF spectrometry (pXRF) is capable of performing rapid and cost-efficient analyses. Indeed, such analyses have recently been applied to cores of organic rocks in the USA in order to acquire geochemical data. The identified geochemical changes over the core sections can be linked with features noted during core examination that relate to the stratigraphy, sedimentology and paleontology of the rocks (Rowe et al., 2012).

The authors have employed thin section petrography to provide a clearer insight into the depositional environment of Upper Viséan to Lower Namurian (Carboniferous) mudstone dominated strata covered by core. Moreover, to focus on the complex relationship between microfacies changes and changes in the mineralogy of the sedimentary rocks, the petrographic data have been integrated with data obtained from pXRF, which helps to recognise sequence variation through changes in the inorganic geochemical composition.

Geological setting

The study reported herein has been undertaken on a core section of Upper Viséan to Lower Namurian sedimentary rocks from Zuid-Limburg, the Netherlands, which is situated within the eastern part of the Campine Basin. The basin lies to the north and east of the London-Brabant Massif (an important high during Carboniferous times) and forms part of the northwest European Carboniferous Basin (Kombrink et al., 2008a). Strata associated with this Variscan foreland basin can be traced along

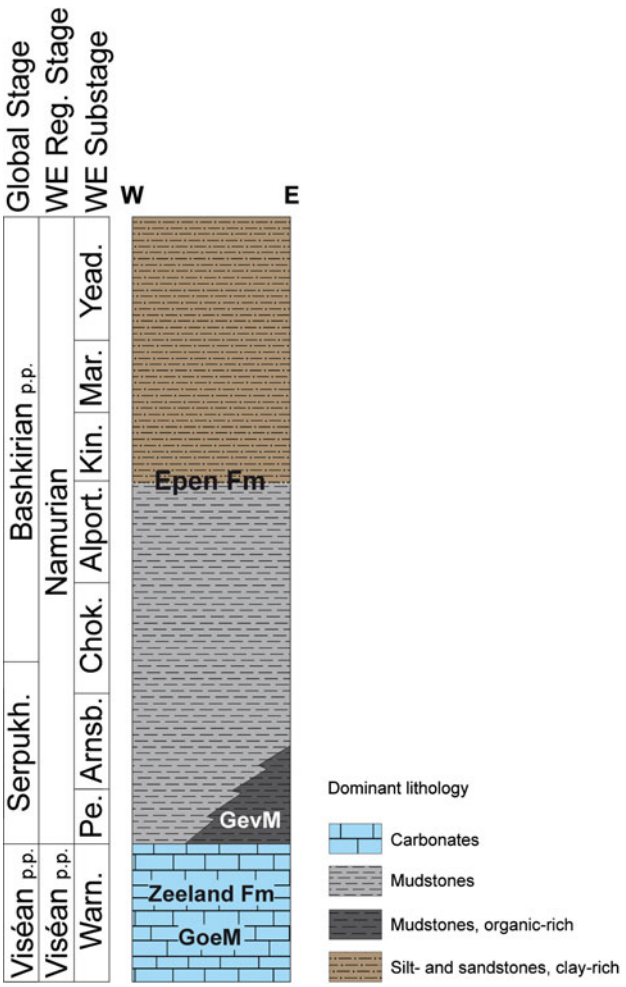

Fig. 1. Generalized chrono- and lithostratigraphic settings for the studied area. Epen Fm, Epen Formation; GevM, Geverik Member; Zeeland Fm, Zeeland Formation; GoeM, Goeree Member. Chronostratigraphy: Serpukh., Serpukhovian; Warn., Warnantian; Pe., Pendleian; Arnsb., Arnsbergian; Chok., Chokierian; Alport., Alportian; Kin., Kinderscoutian; Mar., Marsdenian; Yead., Yeadonian; p.p., pro parte; Reg., Regional. Lithostratigraphy modified after Kombrink et al. (2010). Chronostratigraphy after Davydov et al. (2012).

an arc ranging from Poland in the east to Germany, the Netherlands, Belgium and Great Britain in the west.

In general, deposition in the basin was influenced to a great extent by the onset of the Variscan orogeny (Kraft, 1992; Mathes-Schmidt, 2000). During the Tournaisian and Viséan (= 'Dinantian'), platform carbonates and fine-grained siliciclastic material accumulated in the basin, whereas siliciclastic deposits of variable grain size prograded into the Campine Basin during Early Namurian times. Basin fill exceeded basin subsidence later in the Namurian, resulting in the onset of paralic settings (Kraft, 1992).

The stratigraphy for the onshore southern Netherlands area (Van Adrichem Boogaert & Kouwe, 1993) assigns the Upper Viséan to Lower Namurian strata to the Goeree Member of the Zeeland Formation (Carboniferous Limestone Group) and to the Epen Formation (Limburg Group), respectively (Fig. 1).

https://doi.org/10.1017/njg.2015.25 Published online by Cambridge University Press

The Upper Viséan Goeree Member of the Zeeland Formation comprises a succession of black limestones, which, in some cases, show a fairly high degree of silicification. Mathes-Schmidt (2000) and Van Amerom (1986) provide detailed information and a summary profile of the studied Upper Viséan carbonates. The Upper Viséan to Lower Namurian strata within the study area have been influenced by a fall in sea level, which marks the Viséan–Namurian boundary.

The Namurian rocks belong to the Epen Formation. The Geverik Member corresponds to the basal successions of the Epen Formation and consists of bituminous black shales. It is characterised by high gamma American Petroleum Institute (API) values ranging from 300 to 500 (Van Adrichem Boogaert & Kouwe, 1993), which indicate that the shales contain high levels of radiating elements, i.e. U, Th and K. Furthermore, the lack of *in situ* benthic fauna and the presence of abundant organic matter point to deposition from suspension in an anoxic marine basin with restricted circulation. Occasional intercalated, graded siltstones/sandstones and limestone laminae are the products of distal turbidites.

Overlying the Geverik Member are dark grey to black mudstones of the Epen Formation. Van Adrichem Boogaert & Kouwe (1993) note that the upper boundary of the formation is diachronous and becomes younger from south (Namurian B–South Limburg) to north (Early Westphalian A–central onshore, well Nagele 1), which corresponds to a northwards prograding delta system. Detrital material is most likely to have come from the south, from along the London-Brabant Massif and/or the Variscan thrust belt.

Material and methods

The studied core section from a well drilled in South Limburg, the Netherlands ranges from 1058 m to 726 m (Fig. 2) and covers Upper Viséan to Lower Namurian successions containing abundant organic matter. The occurrence of goniatites confirms the placement of the Viséan–Namurian boundary at 980.5 m (D. Korn, pers. comm., 2011), which is in accordance with the results of Van Amerom (1986). Samples taken from the core section have been subjected to analysis by petrography and pXRF.

A detailed core description (1:40 scale) produced via WellCAD has been employed to identify the main lithologies in the core section, which were sampled for petrographical analysis. The locations of these samples in the core section are shown in Fig. 2. Measurements of the core section by pXRF have also been integrated into the dataset, with a focus on the Lower Namurian mudstone-dominated strata.

Thin section petrography

Eighty large thin sections (75 mm × 100 mm) and 18 small thin sections (28 mm × 48 mm) were prepared and examined (Fig. 2). The preparation of the thin sections was executed following the procedure advocated by Reed & Mergner (1953). The fissile mudstones were stabilised using epoxy resin (RECKLI-Injektionsharz EP) prior to slabbing and thin section preparation.

Classification of the carbonate rocks is after Dunham (1962). However, to avoid confusion with siliciclastic rocks, the term 'lime mudstone' refers to micritic deposits (= mudstones of Dunham, 1962). Classification of the siliciclastic mudstones follows the informal, but generally accepted, textural-based scheme that has been successfully applied during the past 25 years by Schieber (1989, 1999), Caplan & Bustin (2001), Röhl et al. (2001), Loucks & Ruppel (2007), Trabucho-Alexandre et al. (2012) and Könitzer et al. (2014).

Interpretation of the petrographical data has led to the recognition of six microfacies associations (MFA) over the core section.

Portable X-ray fluorescence

pXRF analyses have been undertaken by a Niton Model XL3t analyser, with 592 points over the core section being analysed. On average, a lithological representative core sample was analysed every 50 cm, although some analyses were only 10 cm apart over the Lower Namurian organic strata (844–1023 m), whilst others were up to 7 m apart over the 726–844 m and 1023–1058 m intervals.

The pXRF analyser operates at 50 kV and 0.1 mA, and employs a miniature X-ray tube with an Ag anode fitted with multiple filters. Geometrically optimised large drift detector (GOLDD) technology provides optimum X-ray detection for a wide range of elements, e.g. magnesium to uranium. At the start, during and end of the analyses, the CRM OU-6 (Penrhyn Slate; Potts & Kane, 2003) was analysed at regular intervals to correct for instrument drift. For the determination of element concentrations about 0.5 wt% (5000 ppm) or greater (lithotype depending, i.e. magnesium has detection limits of 1–2 wt% oxide), the Mining mode is used. However, magnesium (Mg) can be detected only in rocks where Mg levels exceed 2 wt% oxide and due to the lack of an appropriate standard, any Mg data acquired via pXRF analyses should be regarded as semi-quantitative at best.

Element data are presented chiefly as absolute values, either in parts per million (ppm) or in wt% oxide, but are sometimes also given either as element ratios or in the form of log base ten values (e.g. CaO), which can help in identifying any stratigraphic/spatial trends within the geochemical dataset. The amount of uranium linked with organic matter (U_{org}) is calculated using the following equation:

$$U_{org} = (U/Al) \times (U/Zr) \quad (1)$$

Uranium has been normalised against aluminium (Al) and zirconium (Zr) to take into account the quantity of this

https://doi.org/10.1017/njg.2015.25 Published online by Cambridge University Press

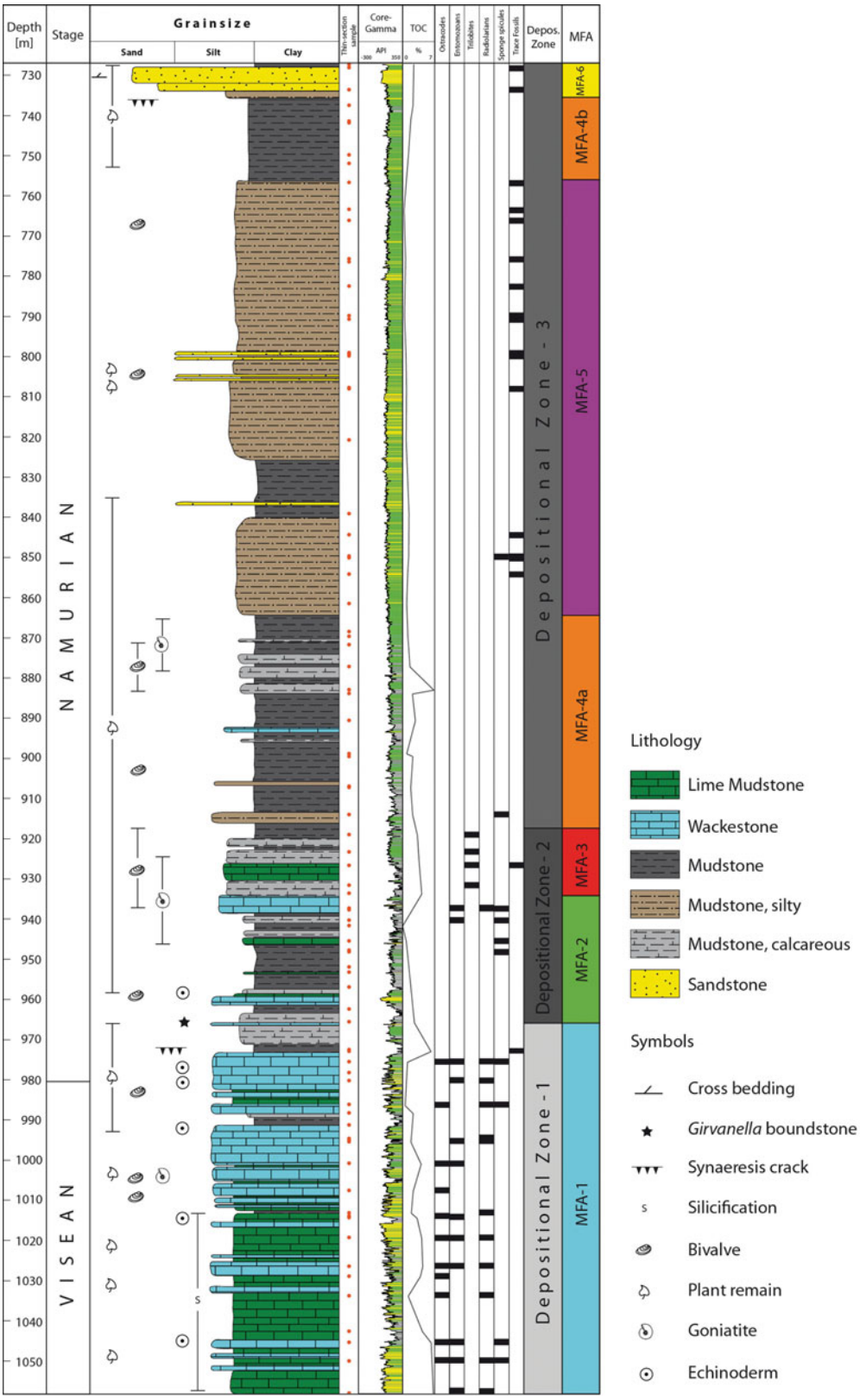

Fig. 2. Simplified lithofacies and associated depositional zones as well as microfacies associations of the studied core section. Additional information includes core gamma, total organic carbon (TOC), and fossil content as observed in thin sections.

https://doi.org/10.1017/njg.2015.25 Published online by Cambridge University Press

Table 1. Overview of the different microfacies associations (MFA) including microfacies types.

Facies	MFA–1	MFA–2	MFA–3	MFA–4	MFA–5	MFA–6
Entomozoan–bearing lime mudstone	+					
Entomozoan–bearing wackestone	+					
Calcareous mudstone	–	–		–		
Laminated mudstone	–					
Sandy lenticular mudstone		+	–			
Lenticular mudstone		–		+	–	
Dark lime mudstone		–	–			
Argillaceous wackestone		–				
Fossiliferous argillaceous wackestone			+			
Lenticular laminated mudstone				+		
Silty burrowed–laminated mudstone					+	
Sandstone					–	
Silt– and sandstone						+

Occurrence: +, dominant; –, minor.

element, which is associated with clay minerals and heavy minerals, respectively.

To ensure the accuracy and reliability of the geochemical data acquired via pXRF, the data were compared with data obtained from lithological representative samples via analyses by a bench-top spectrometer (Spectro Xepos AMETEK). Sample preparation for these analyses involved grinding 4.0 g of dried rock for 4 min in a planetary Monomill (Pulverisette 6 FRITSCH) and then pressing the resultant powder into pellets of 32 mm diameter. Empirical calibration for the major element, minor element and trace element data was created by analysing the same CRM OU-6 (Penrhyn Slate) as was used for the pXRF analysis.

Interpretation of the geochemical data acquired by the pXRF analyses has allowed a chemostratigraphic zonation to be established for the core section that consists of chemostratigraphic units and subunits.

Principal component analysis

Chemostratigraphy entails the zonation of sedimentary rock successions based on stratigraphic changes in their inorganic geochemistry. The differing geochemical characteristics of the divisions making up the chemostratigraphic zonations reflect variations in the mineralogy of the sedimentary rocks. To determine which minerals control the stratigraphic variations in geochemistry, one needs to establish element–mineral affinities and, in particular, which elements are linked with detrital minerals and which are linked with authigenic minerals. A zonation based on stratigraphic changes in Ti/Zr values reflects changes in the abundance and distribution of detrital heavy minerals that in turn are associated with provenance changes and so presumably would have a regional extent and thus would form the ideal foundation for a chemostratigraphic zonation. Conversely, stratigraphic changes in CaO concentrations are likely to be linked to changes in the abundance of authigenic carbonate cements, the abundance and distribution of which are frequently independent of stratigraphy and so are of little practical use for establishing chemostratigraphic zonations. In addition, elements may have affinities with more than one mineral. For example, Fe can be associated with pyrite, clay minerals (chlorite) and carbonate minerals like siderite. Pearce et al. (2005) have shown how principal component analysis (PCA) can be used to determine element associations from which element–mineral affinities can be inferred. Svendsen et al. (2007) present a detailed discussion regarding the use of PCA in the context of geochemical data interpretation

Results and discussion

Lithostratigraphy and microfacies associations

Interpretation of the data obtained by the thin section analyses has resulted in the recognition of six microfacies associations (MFA). Fig. 2 shows the distribution of the MFAs over the core section and the locations of the thin section samples. The different varieties of each microfacies association are summarised in Table 1.

Microfacies Association 1 (MFA-1: 1058–966 m) (Fig. 3) Two predominant microfacies make up MFA-1, i.e. a lime mudstone with entomozoan ostracodes (Fig. 3A and 3B) and a wackestone with entomozoan ostracodes (Fig. 3C and 3D), along with two minor varieties, i.e. a calcareous mudstone (Fig. 3E) and a mudstone (Fig. 3F). Ostracodes, and especially the spinose entomozoan types, are a characteristic component of MFA-1 and their presence is one of the characteristics that separate this microfacies

https://doi.org/10.1017/njg.2015.25 Published online by Cambridge University Press

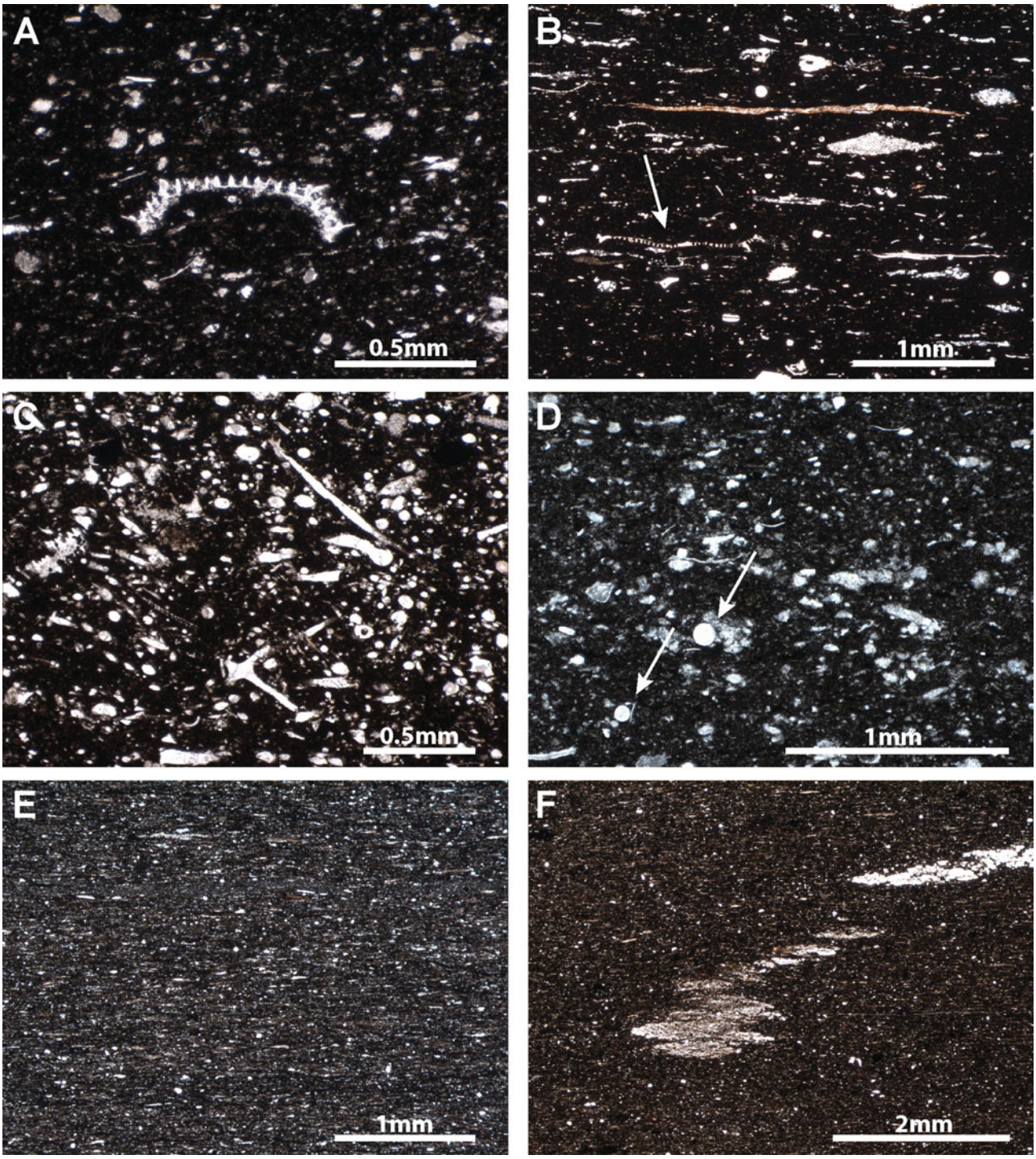

Fig. 3. MFA-1. A. Detailed view of a silicified lime mudstone shows disarticulated entomozoan valve. Note the characteristic spinose shell surface (1045.27 m). B. Calcareous mudstone with abundant flattened bioclasts. Arrow highlights position of entomozoan valve (980.10 m). C. Wackestone with abundant sponge spicules. Note presence of tetraxon and monaxon spicules (975.35 m). D. Another example of a wackestone. It shows two perfectly round radiolarians (arrows) and very fine bioclasts (1.019.20 m). E. This calcareous mudstone shows a relatively strong silicification and a relict lamination (?bioturbation) as well as a lack of larger components (1028.75 m). F. Stacked pattern of silt-filled Planolites *burrows within a mudstone. Note homogeneous mudstone fabric (972.75 m).*

https://doi.org/10.1017/njg.2015.25 Published online by Cambridge University Press

association from MFA-2. The top of MFA-1 is defined by a 40 cm thick *Girvanella* boundstone.

The individual lime mudstone beds range in thickness from 3 to 150 cm and they alternate with wackestone beds of 3–230 cm in thickness. Towards the top of MFA-1, the frequency of lime mudstones decreases, whereas wackestones become more common. Below 1014 m the predominant lime mudstones and wackestones are conspicuously silicified. The wackestones above this depth lack a comparable degree of silicification. In many cases the lime mudstone and wackestone microfacies grade vertically into a mudstone microfacies. Although the two mudstone microfacies (calcareous mudstone and mudstone) are of minor importance, their frequency increases towards the top of MFA-1 as well: bed thicknesses range from 3 to 30 cm and the thickest beds occur above 1014 m, where wackestones are predominant.

The limestone beds show fine parallel laminae made up of silt-grade bioclastic components and have well-defined, erosional contacts with the underlying lithologies. Although the lime mudstones and wackestones contain different amounts of bioclastic components, they resemble each other texturally, with the lower part of a bed chiefly comprising silt-grade bioclasts 'floating' in a dark micritic matrix, whilst the upper part commonly has fine parallel alternating clay and bioclastic laminae. Microfossils 'floating' within the matrix and the larger bioclasts include small amounts of bivalves, ostracodes and radiolarians. Apart from smooth-valved ostracodes, the characteristic spinose valves of pelagic ostracodes (Entomozoacea) are ubiquitous within the different limestone facies – ostracode valves mostly are disarticulated, with rare articulated ostracodes. Detrital grains were not recognised.

Calcareous mudstones and mudstones are scarce in MFA-1, but where present both have millimetre-scale alternating dark and light laminae. The dark laminations are made up of wavy aggregates of silt-grade flakes within a dark argillaceous matrix and clay-dominated laminae. Also some relict to diffuse laminations were observed. The biogenic and non-biogenic components are similar to those seen in the lime mudstones and wackestones, and silt-grade pyrite grains seem to be common in dark mudstones. Mudstones are predominant over the 991–988 m interval in MFA-1, which has significantly higher gamma API values (>300) than adjacent successions. Its thickness, lithology and position of the interval close to the Viséan–Namurian boundary at 980.5 m suggests it could represent the isochronous Upper Viséan *Actinopteria* Black Shale Event, which has been well documented in the Rhenish Mountains and the Harz Mountains in Germany (Ruprecht, 1937; Amler, 2006; Korn, 2008; Nyhuis et al., 2015). However, the eponymous bivalve *Ptychoparia* (*Actinopteria*) *lepida* (Goldfuss) was not observed in this interval, possibly because either strong shearing/tectonism destroyed the valves or the shell-bearing layers were lost via erosion. The thin section relating to the interval shows that the lithology has a homogeneous fabric and contains a moderate amount of small bioclasts, corresponding to the *Actinopteria* Black Shale microfacies type MF-2 (dark calcareous mudstone) as described by Nyhuis et al. (2015).

Macroscopic fossils noted within MFA-1 include goniatites, bivalves, disarticulated crinoid columnals and wood fragments, the latter always being preserved as thin coaly imprints on bedding planes.

Microfacies Association 2 (MFA-2: 966–934 m) (Fig. 4) Three different mudstone microfacies make up MFA-2, i.e. a sandy lenticular mudstone (Fig. 4A and 4B), a lenticular mudstone (Fig. 4C and 4D) and a calcareous mudstone, along with two different limestone microfacies, i.e. a dark lime mudstone (Fig. 4E) and an argillaceous wackestone (Fig. 4F). The sandy lenticular mudstones are the most common microfacies and are predominant between 958 and 946 m. Bed thickness ranges from 2 to 220 cm.

The two lenticular mudstone microfacies are distributed throughout MFA-2, whilst the calcareous mudstone, argillaceous wackestone and dark lime mudstone microfacies tend to be most common between 946 and 934 m. Scarce reworked entomozoan valves are present in the latter two microfacies. The apparent random distribution of the five microfacies over interval MFA-2, coupled with the overall predominance of clay, are the main characteristics that set this microfacies association apart from MFA-1. The bed thicknesses of the various MFA-2 microfacies are quite variable and range from the centimetre to the decimetre scale.

All the above microfacies contain some well-sorted, angular to subangular, silt- to sand-grade detrital grains. A characteristic feature of the common sandy lenticular mudstone microfacies is, as the name implies, the presence of horizontal lenses comprising clay and silt-grade grains that sit in a dark argillaceous matrix. Sand-grade grains occur within both the matrix and the lenses. However, the abundance of the argillaceous matrix is somewhat variable and locally the lenses become much more common, with little matrix remaining, whilst in some cases the individual lenses become amalgamated. Sand-grade grains are much scarcer in the lenticular mudstone microfacies, which nevertheless has a similar appearance to the sandy lenticular mudstone microfacies. The boundaries between this latter microfacies and the other microfacies are usually well defined.

MFA-2 does not possess large numbers of microscopic biogenic components and the only fossils recognised in thin sections are sponge spicules, which are relatively frequent in the calcareous mudstone, argillaceous wackestone and dark lime mudstone microfacies that are common between 946 and 934 m. Despite hand specimens collected from these microfacies that split quite readily along well defined partings, there is little or no evidence for the presence of laminae observed in thin section. The three microfacies are characterised by locally common detrital sand-grade grains, which are well sorted and

https://doi.org/10.1017/njg.2015.25 Published online by Cambridge University Press

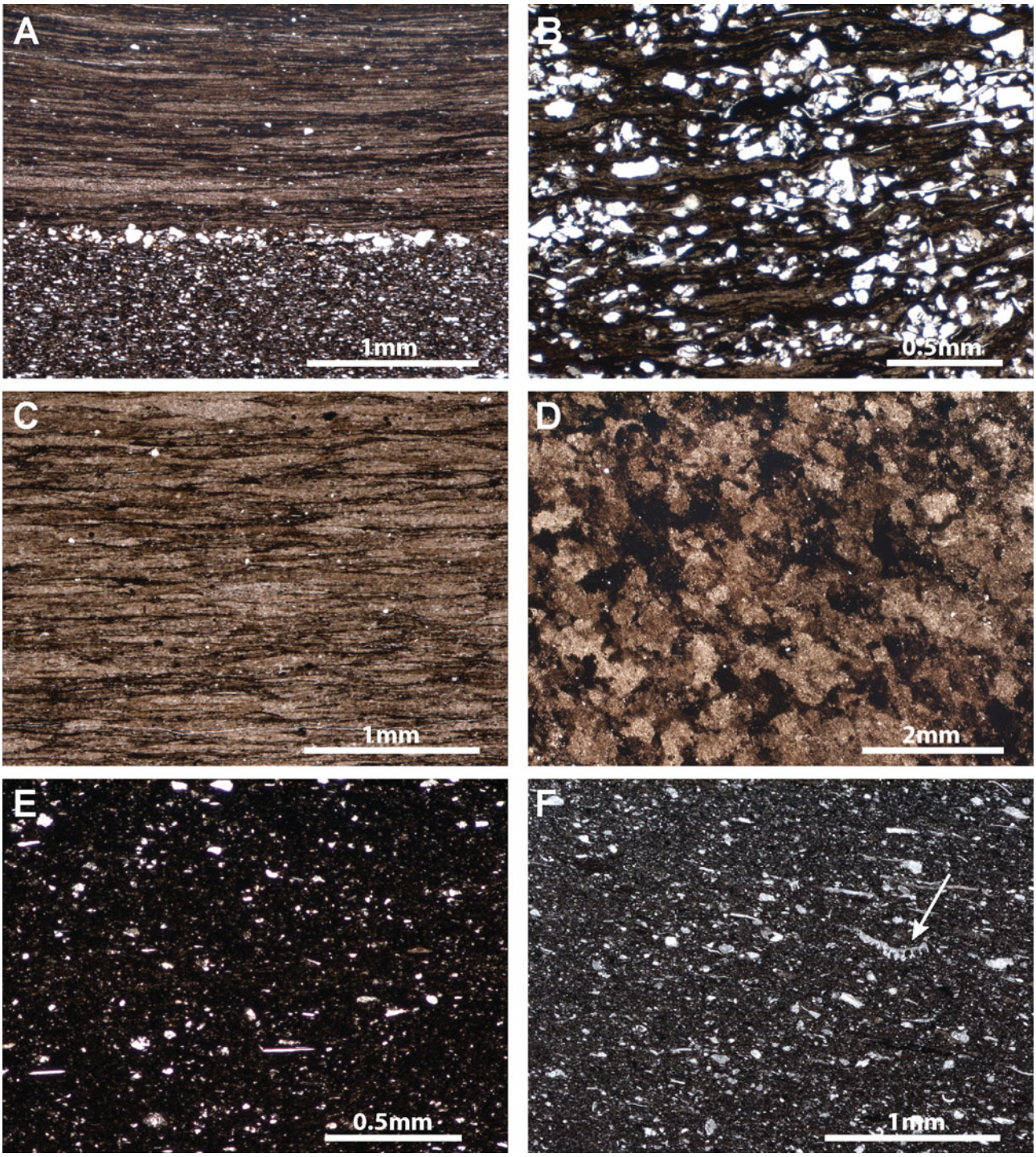

Fig. 4. MFA-2. A. Erosional contact between sandy lenticular mudstone (bottom) and lenticular mudstone (948.10 m). B. Same sample as A shows well-sorted subangular sand grains interbedded within lenticular mudstone. Apart from the large amount of detrital grains, monaxon sponge spicules (bright straight structures) are the main components. C. A large number of clasts comprising clay and silt-grade grains results in a lenticular mudstone fabric. Note the irregularly distributed minor amount of sand grains (951.84 m). D. Section parallel to bedding (same sample as C) exhibiting interconnection of lenses comprising clay and silt-grade grains that show an irregular outline. Dark spots are intercalations of organic-rich matter. E. This dark lime mudstone shows a minor amount of detrital grains and sponge spicules within a clay-rich micritic matrix (940.20 m). F. Argillaceous wackestone with numerous fine-grained bioclasts. Note (reworked) entomozoan valve (arrow) (937.16 m).

https://doi.org/10.1017/njg.2015.25 Published online by Cambridge University Press

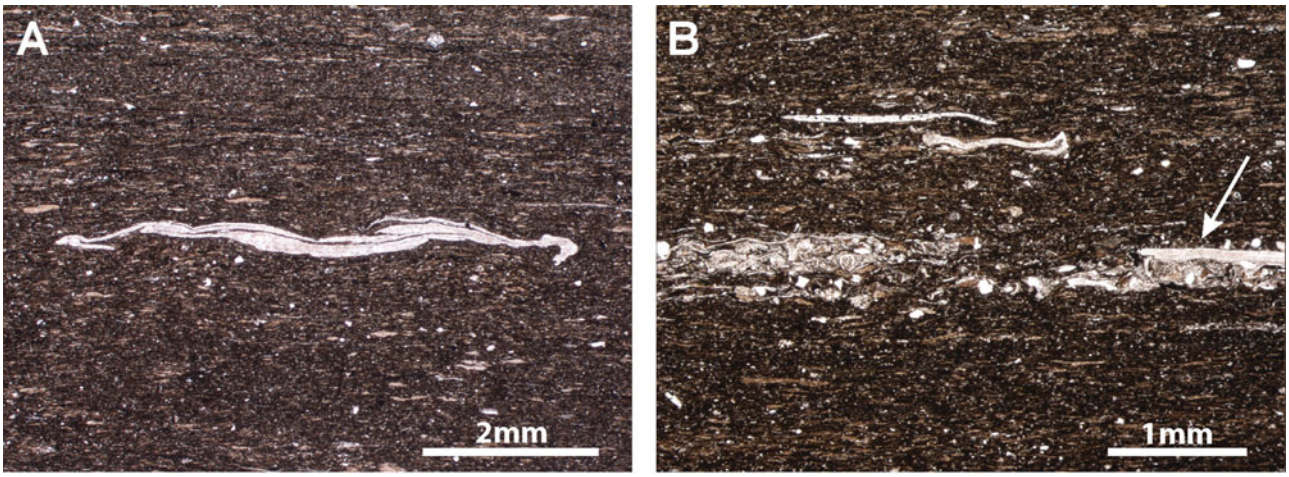

Fig. 5. MFA-3. A. Cross-section of a well-preserved articulated trilobite thorax within a fossiliferous mudstone. Note typical shepherd's hook structure of trilobite and homogenous to faintly laminated fabric (931.40 m). B. Fossiliferous mudstone with intercalation of bioclastic lamina. Lamina disruption is the result of burrowing. Note bivalve shell (arrow) within bioclastic lamina (926.43 m).

subangular, and fairly frequent sponge spicules 'floating' in their matrices, as in the calcareous mudstone microfacies of MFA-1.

The macrofossil assemblage of MFA-2 is comparable to that of MFA-1, although bivalves are not as common in MFA-2.

Microfacies Association 3 (MFA-3: 934–917 m) (Fig. 5) The microfacies of MFA-3 are not that different from the sandy lenticular mudstone microfacies of MFA-2 in terms of their matrix and components. However, the dominant facies of MFA-3, i.e. the fossiliferous calcareous mudstone microfacies (Fig. 5A and 5B), is characterised by having a heterogeneous fabric and *in situ* benthic fauna. These features allow a differentiation of MFA-3 from MFA-2. The thicknesses of the beds belonging to this microfacies range from the decimetre to metre scale. The fossiliferous calcareous mudstone microfacies is intercalated with beds of dark lime mudstone, plus a few beds of sandy lenticular mudstone (both decimetre scale), similar to those of MFA-2.

The fossiliferous calcareous mudstone microfacies contains common silt-grade quartz grains, although they are distributed throughout the mudstone matrix rather than being concentrated in lenses, as in MFA-2. Local thin bioclastic laminae are another characteristic feature of these mudstones, although some laminae have been disrupted and show a downward orientated drag of bioclasts (Fig. 5B). The microfacies additionally contains frequent disarticulated trilobite shells, although articulated specimens are rarer, but all are orientated parallel to bedding. Scarce faecal pellets have also been observed in the mudstones, which contain fine calcareous bioclasts of uncertain origin.

Macroscopic fossils occurring in MFA-3 include coaly fragments of wood, goniatites and bivalves.

Microfacies Association 4 (MFA-4a: 917–864 m; MFA-4b: 756–735 m) (Fig. 6) MFA-4 occurs twice over the core section, the deeper occurrence being termed MFA-4a and the overlying occurrence being termed MFA-4b. MFA-4a is distinguished from MFA-3 below by the lenticular fabric of the two predominant mudstone microfacies, i.e. the lenticular mudstone microfacies (Fig. 6A to 6C) and the lenticular laminated mudstone microfacies (Fig. 6C). Both microfacies alternate on a centimetre to metre scale. MFA-4a and MFA-4b share the same microfacies although the MFA-4b lenticular mudstone microfacies has slightly more detrital quartz grains (Fig. 6C and 6D). The 884.00–865.55 m interval within MFA-4a contains the last abundant calcareous mudstone beds (on a decimetre scale) encountered up-sequence, whereas the last goniatites recorded over the core section come from the 876.00–865.65 m interval, the top of which represents the upper boundary of MFA-4a.

The fabric of the laminated mudstones is defined by lenticular laminae of silt-grade grains alternating with clay intercalations on a sub-millimetre scale, whereas the lenticular mudstones lack the clay intercalations. The calcareous MFA-4a mudstones are comparable to those of MFA-2, with most having a lenticular fabric.

With respect to both microfacies associations, but especially MFA-4b, some silt-grade detrital grains are found either within the lenses comprising clay and silt-grade grains or in the argillaceous matrix. Very few microscopic biogenic components have been recorded in MFA-4a and MFA-4b, apart from one sponge spicule-bearing sample collected from close to the boundary with MFA-3 and the small bioclasts found within the calcareous MFA-4a mudstones.

The types of macroscopic fossils preserved on the bedding planes within MFA-4a and MFA-4b do not differ markedly from those identified within MFA-3, although bivalve fossils are predominant and the coaly remains of wood fragments are common.

https://doi.org/10.1017/njg.2015.25 Published online by Cambridge University Press

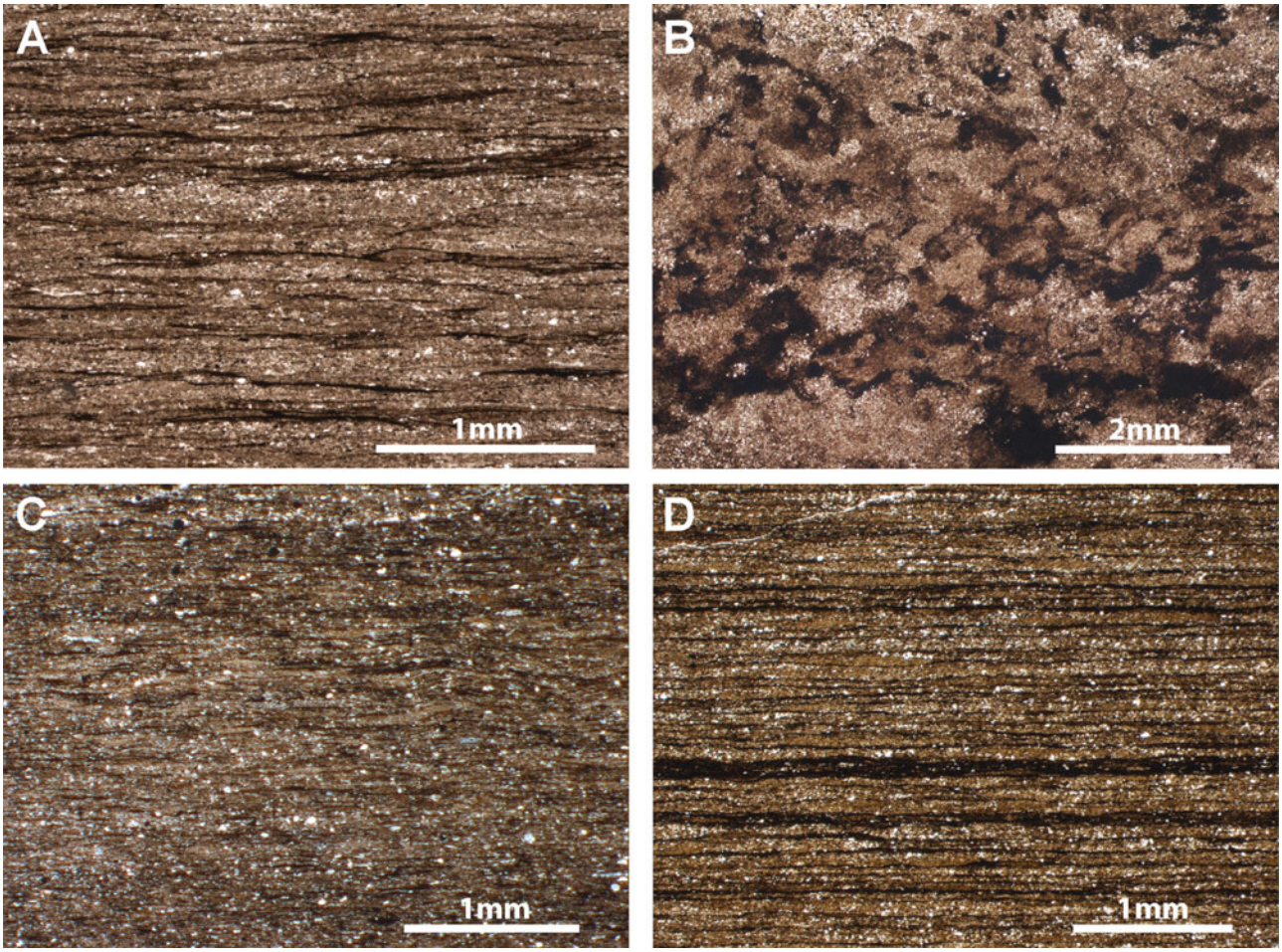

Fig. 6. MFA-4. A. This lenticular mudstone shows a strong degree of sediment compaction that causes an amalgamation of lenses comprising clay and silt-grade grains (869.40 m). B. Section parallel to bedding (same sample as A) exhibiting irregular outline of lenses comprising clay and silt-grade grains. Dark areas represent the clay-rich matrix. C. Slightly undulating lenticular mudstone with moderate amount of fine detrital quartz grains (740.80 m). D. Well-laminated lenticular mudstone that is composed of an alternation of lenses comprising clay and silt-grade grains and clay-dominated laminae (737.15 m).

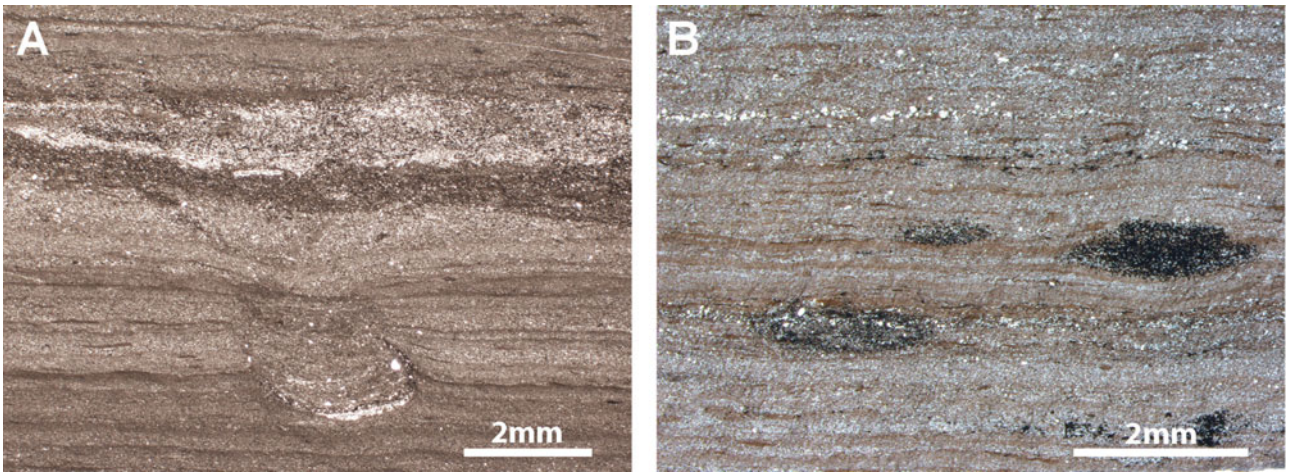

Fig. 7. MFA-5. A. Teichichnus *burrow with characteristic retrusive arrangement of spreiten within a silty burrowed-laminated mudstone. Note that the burrow is cut off at its top by an erosional surface (789.62 m). B. Pyritized* Planolites *burrows within a silty burrowed-laminated mudstone. Note differential compaction around burrows (763.00 m).*

https://doi.org/10.1017/njg.2015.25 Published online by Cambridge University Press

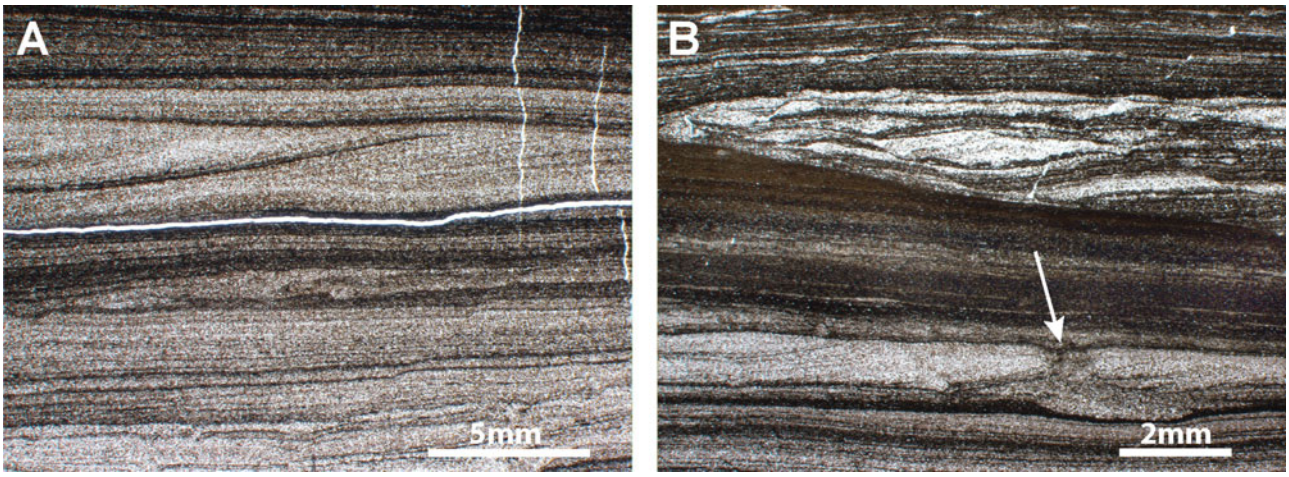

Fig. 8. MFA-6. A. Cross-stratified argillaceous siltstone. Vertical bright structures are quartz-filled fractures. Horizontal void is a preparation artefact (733.25 m). B. Same sample as A shows a burrow (arrow) within cross-laminated argillaceous siltstone. Note sharp erosive contact between cross-laminated sand-rich layer (bright) and clay-rich laminated layer (dark).

Microfacies Association 5 (MFA-5: 864–756 m) (Fig. 7) MFA-5 occurs between MFA-4a and MFA-4b and chiefly comprises bioturbated to laminated silty mudstones (Fig. 7A and 7B), whilst local sandstone intercalations, some of which are bioturbated, and mudstones occurring between 840 and 826 m are of lesser importance. The characteristics distinguishing MFA-5 from MFA-4a and MFA-4b are the presence of burrows and the absence of lenticular fabrics, although the evidence from one thin section taken from the mudstones indicates they might have silty lenses.

The laminations are defined by silty/sandy laminae alternating with clay laminae, the boundaries between the individual laminae being well defined, whilst a marked colour contrast between the finer and coarser laminae give the silty mudstones a varved appearance. In some cases, the laminae show downlapping, which is interpreted as low-angle cross-stratification. Various, but essentially simple, trace fossils, such as *Skolithos*, *Teichichnus* and *Planolites*, are present within this microfacies. Even though the vertical *Skolithos* burrows typically cut through several laminations, the burrows are not common enough to destroy the sedimentary structures completely, with the same being true for the *Teichichnus* burrows. The upper parts of these burrows tend to be truncated by erosional surfaces. In contrast, the smaller *Planolites* burrows seem to be confined to the argillaceous sections and are frequently pyritised, which has not affected the vertical burrows. The local sandstones mentioned above show wavy lamination, cross-bedding, soft-sediment deformation and the mentioned burrows. The detrital grains making up the sandstones are well sorted and subangular, and consist mostly of quartz, although some feldspar grains have been noted and the sandstones also have small amounts of clay.

Macroscopic fossils are very rare within MFA-5 and are limited to occasional single bivalve specimens. Coaly imprints of wood fragments are frequent, but are not as common as in the adjacent MFA-4a and MFA-4b microfacies associations.

Microfacies Association 6 (MFA-6: 735–727 m) (Fig. 8) MFA-6 represents the topmost microfacies association recognised over the studied core section, and consists of siltstones and sandstones with thin mudstones (Fig. 8A and 8B). The microfacies association reflects a distinct coarsening of grain size with respect to MFA-5, although both microfacies associations have similar sedimentological and textural features. Bed thicknesses range from 20 to 50 cm.

The siltstones and sandstones show ripple laminations and locally are moderately argillaceous, their contacts with the mudstones always being well defined and erosional. Bioturbation is reflected by the presence of sand-filled lenses within the mudstones (commonly below the surface of a single bed) and by vertical structures within the siltstones and sandstones that have disrupted the laminae.

The only macrofossils present within MFA-6 are the coaly imprints of wood fragments.

Chemostratigraphy (Figs 9 and 10)

Interpretation of the inorganic geochemical data acquired from the core section via pXRF has resulted in the recognition of three chemostratigraphic units and 13 chemostratigraphic subunits. The main geochemical characteristics of these divisions are described below. These characteristics were used to define the boundaries between the various divisions (Fig. 9).

Unit 1 (1058–966 m) Unit 1 is the deepest chemostratigraphic unit identified. It is equivalent to MFA-1 and corresponds to the Goeree Formation. It is characterised by higher Si/Zr values, log Ca levels, U_{org} levels and U levels than Unit 2, as well as lower

https://doi.org/10.1017/njg.2015.25 Published online by Cambridge University Press

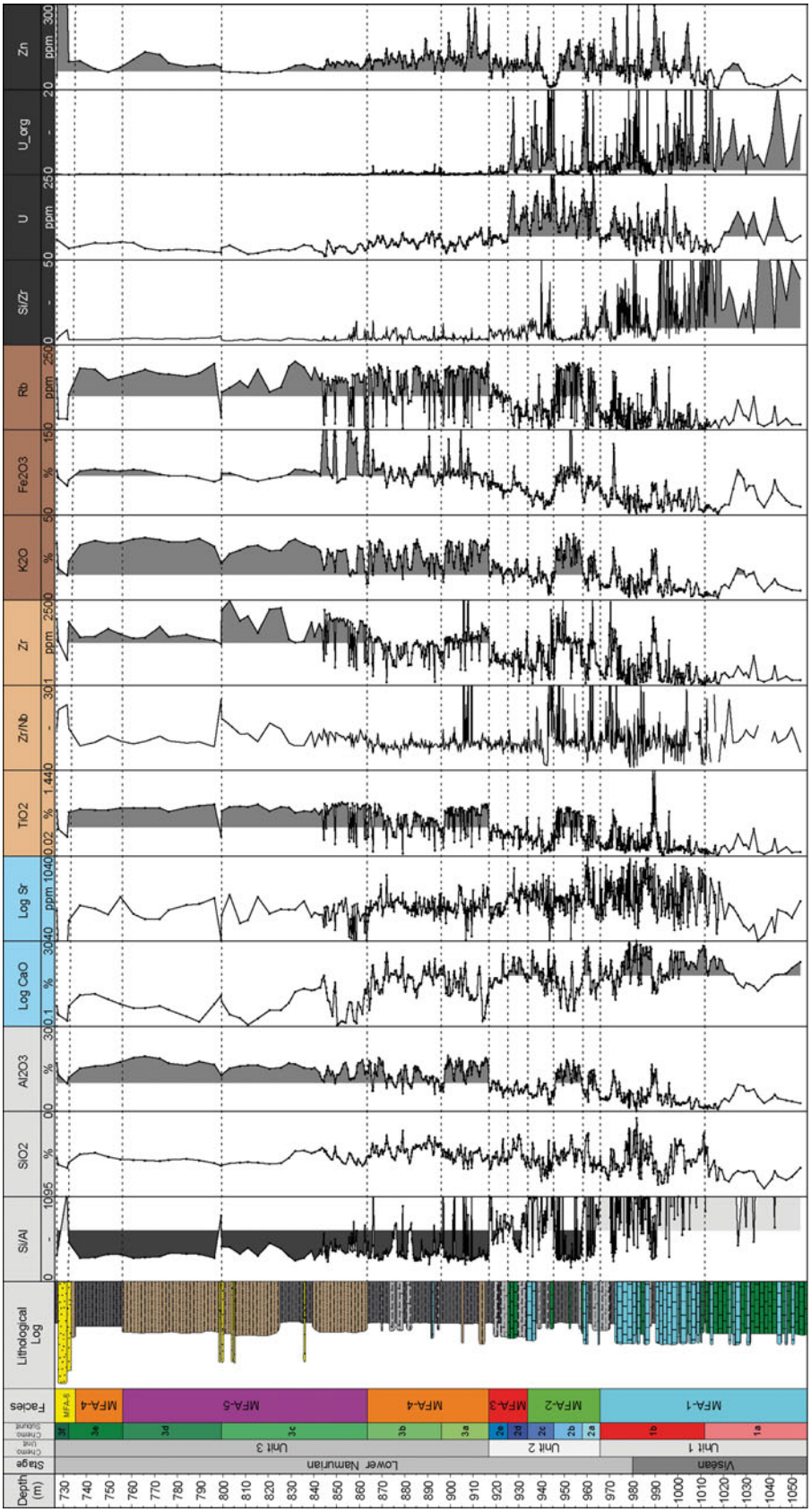

Fig. 9. Simplified lithofacies, microfacies associations, chemostratigraphical units, subunits, and corresponding dataset obtained by portable XRF of the studied core section.

https://doi.org/10.1017/njg.2015.25 Published online by Cambridge University Press

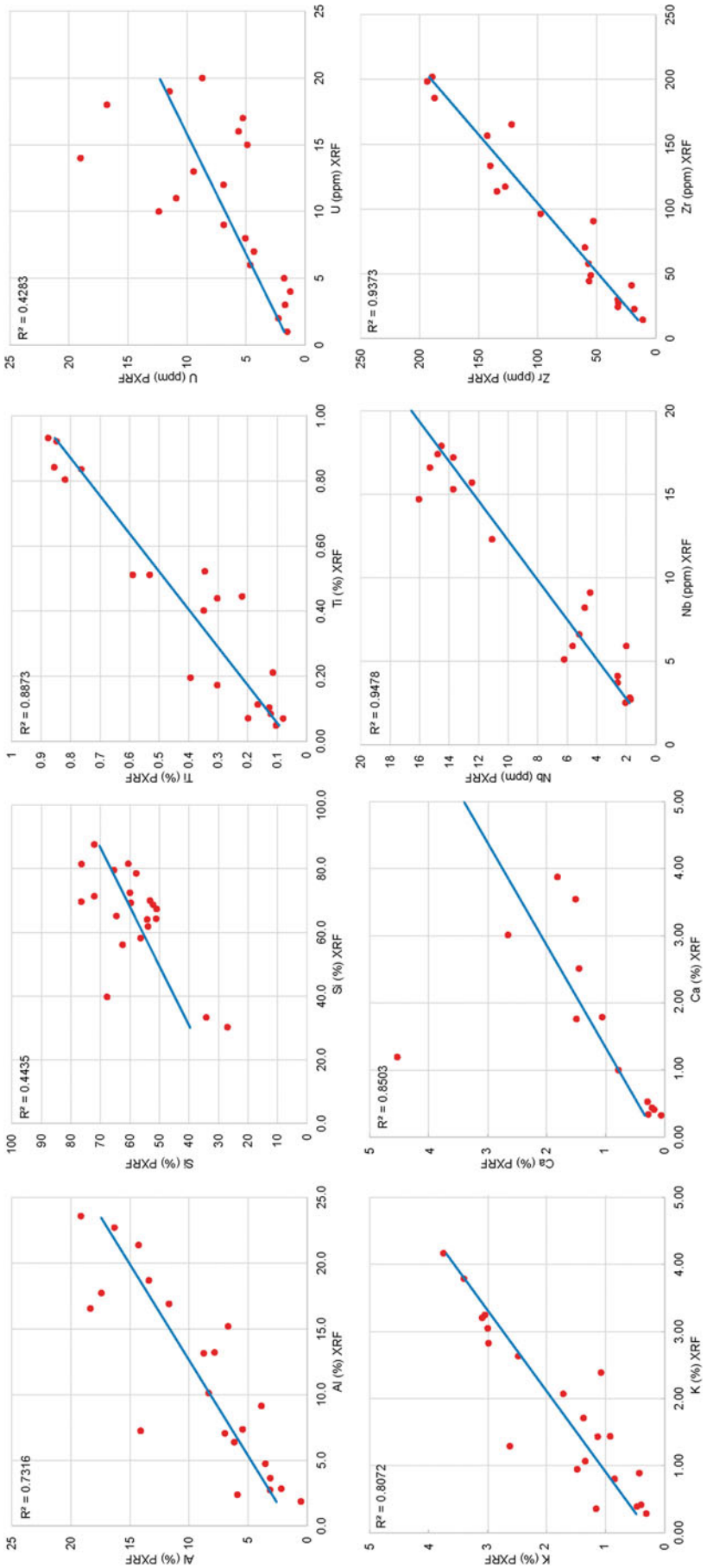

Fig. 10. Benchtop XRF (x-axis) versus portable XRF (y-axis) data highlights the deviation between these different methods.

https://doi.org/10.1017/njg.2015.25 Published online by Cambridge University Press

Al, Fe, Ti, K, Zr and Rb levels. Unit 1 has been divided into Subunits 1a and 1b, as follows:

Subunit 1a (1058–1012 m): characterised by lower Si/Zr values, lower log Ca levels and higher Al, Fe, Ti, U and K levels than Subunit 1b.
Subunit 1b (1012–966 m): characterised by higher Si/Zr values, higher log Ca levels and lower Al, Fe, Ti, U and K levels than Subunit 1a.

Unit 2 (966–917 m) Unit 2 represents the Geverik Member and is equivalent to MFA-2 and MFA-3. The unit is characterised by lower Al, Fe, Ti, Zn and Rb levels, higher Si/Zr values and higher log Ca, U and U_{org} levels than Unit 3, and has been divided into Subunits 2a to 2e, as follows:

Subunit 2a (966–958 m): characterised by higher Si/Zr values, higher log Ca and U_{org} levels and lower Ti, K and Rb levels than Subunit 2b.
Subunit 2b (958–945 m): characterised by higher Al, Fe, Ti, K, Zr and Rb levels than Subunit 2c, as well as lower log Ca and U_{org} levels.
Subunit 2c (945–934 m): characterised by lower Si, Log Ca, K and Fe levels, plus higher U and U_{org} levels, than Subunit 2d. The boundary between Subunits 2c and 2d coincides with the MFA-2–MFA-3 boundary.
Subunit 2d (934–925 m): characterised by lower Zr and Rb levels, along with higher log Ca, log Sr, U and U_{org} levels, than Subunit 2e.
Subunit 2e (925–917 m): characterised by higher Zr and Rb levels, as well as lower log Ca, log Sr, U and U_{org} levels, than Subunit 2d.

Unit 3 (917–726 m) Unit 3 is the topmost unit recognised. It corresponds to the Epen Formation and includes MFA-4 to MFA-6. It is characterised by higher Al, Fe, Ti, Zn and Rb levels, lower Si/Zr values and lower log Ca, U and U_{org} levels than Unit 2, and has been divided into Subunits 3a to 3f, as follows:

Subunit 3a (917–896 m): characterised by higher Al, Ti, Zr and Rb levels and lower Si levels than Subunit 3b. The base of Subunit 3a coincides with the MFA-3–MFA-4 boundary.
Subunit 3b (896–864 m): characterised by lower Al, Ti, Zr and Fe levels, as well as higher log Ca, log Sr and Si levels, than Subunit 3c, with the Subunit 3b–3c boundary coinciding with the boundary between MFA-4 and MFA-5.
Subunit 3c (864–799 m): characterised by lower Rb and Zr levels and higher Zr, log Ca and Fe levels than Subunit 3d.
Subunit 3d (799–756 m): characterised by lower log Ca, Si, Fe and U levels, plus higher Zn levels, than Subunit 3e.
Subunit 3e (756–732 m): characterised by lower Zr/Nb and Si/Zr values, along with higher log Ca, Ti, Zr, K and Rb levels, than Subunit 3f.
Subunit 3f (732–726 m): characterised by higher Zr/Nb and Si/Zr values, as well as lower log Ca, Ti, Zr, K and Rb levels, than Subunit 3e.

The standard deviation for the Al to Si data acquired by pXRF analyses is below 0.27 and ranges from 0.01 to 0.04 for the Ti to K data, whilst the standard deviation for the minor element and trace element data is higher, e.g. 0.72 (Nb) to 15 (Ba). With respect to the geochemical data obtained via benchtop XRF analyses, the standard deviation for the Al to Si data is below 0.26 and fluctuates between 0.01 and 0.002 for the Ti and K data, with the standard deviation for the minor element and trace element data being between 0.02 (Ta) and 14 (Ba). Comparisons between the two datasets reveal a coefficient of determination between 0.4 and 0.8, which reflects the limitations of the pXRF analyses. The relatively large deviations relating to some element data, such as the U, Al and Si data (Fig. 10), is assumed to be due to the different types of analysed samples and analytical methods employed. For instance, the readings obtained during the pXRF analyses can be affected by slight irregularities on the core sample surfaces, which cause the X-rays hitting these surfaces to have variable angles. In contrast, the samples subjected to benchtop XRF analyses were ground into powders and pressed into pellets, which have flat surfaces devoid of any irregularities. Moreover, these pellets are homogeneous and the area analysed is 32 mm in diameter, resulting in the acquisition of data more representative of the analysed samples than the pXRF data, which has been obtained via spot analyses of around 10 mm diameter on the core sample surfaces.

Element–mineral affinities (Fig. 11)

The eigenvector 1 (EV1) and eigenvector 2 (EV2) values determined for the elements for which data have been obtained were plotted together on a EV1 vs. EV2 binary diagram, which resulted in the recognition of five element associations (see below). Element–mineral affinities based on these associations are described below. These affinities compare well with those presented by Ratcliffe et al. (2010), who studied the inorganic whole-rock geochemistry of fluvio-deltaic sandstones and claystones belonging to the Mungaroo Formation (offshore Australia).

Quartz: This group includes just Si and is characterised by a negative EV1 value and a positive EV2 value. The element invariably has a strong affinity with quartz (SiO_2), but can be associated with other silicate minerals such as feldspar, mica and clay minerals.

Carbonate minerals: This group includes calcium (Ca), magnesium (Mg), manganese (Mn) and strontium (Sr), and is characterised by positive EV1 values and negative EV2 values. Ca, Mg and Mn are usually linked with carbonate minerals, e.g. calcite and dolomite.

https://doi.org/10.1017/njg.2015.25 Published online by Cambridge University Press

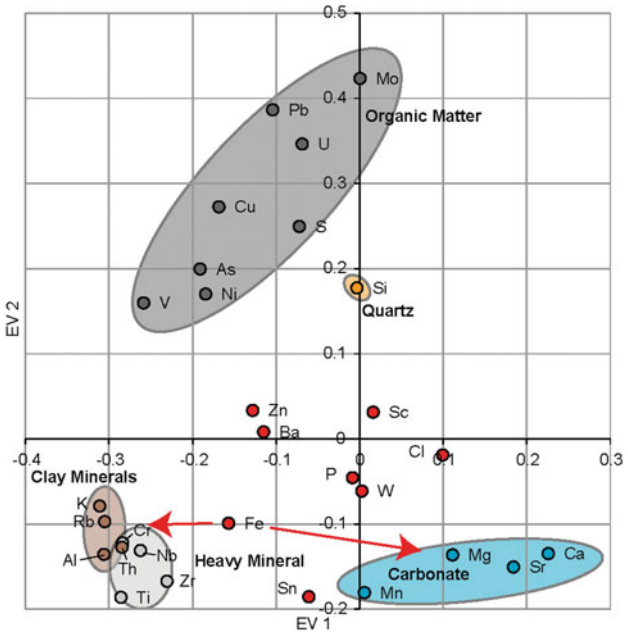

Fig. 11. Eigenvector (EV) cross plots for data derived by principal component analysis and inferred element-mineral affinities.

Heavy minerals: This group includes zirconium (Zr), chromium (Cr), niobium (Nb) and titanium (Ti), and is characterised by negative EV1 values and negative EV2 values. These elements tend to be linked with heavy minerals: Nb and Ti are associated with Ti oxide minerals, Zr has a well-developed affinity with zircon and Cr is linked with heavy minerals like Cr-spinel and tourmaline.

Clay minerals: This group includes aluminum (Al), potassium (K), thorium (Th) and rubidium (Rb), and is characterised by negative EV1 values (lower than those characterising the heavy mineral group) and negative EV2 values. The four elements are usually associated with clay minerals, e.g. chlorite and illite. Th is included in the clay mineral group and Cr is included in the heavy mineral group, but as both elements actually plot between the two groups (Fig. 11), Cr could well belong to the clay mineral group and Th could belong to the heavy mineral group.

Organic matter: This group includes uranium (U), molybdenum (Mo), nickel (Ni), vanadium (V) and sulfur (S), and is characterised by negative EV1 values and positive EV2 values. All these elements typically are linked with organic matter. Their precipitation within the pore fluids is controlled predominantly by the redox state of the fluids. During the decay of organic matter, the elements are reduced, e.g. U(VI) is reduced to U(IV), and as these reduced ions have low solubility and therefore precipitate from the pore fluids (Tribovillard et al., 2006).

Interpretation and discussion

Interpretation of the thin section data and geochemical data acquired from the core section has resulted in the recognition of six microfacies associations, three chemostratigraphic units and 13 chemostratigraphic subunits. By combining these data, three different depositional zones have been identified (Fig. 2), which correspond to the three chemostratigraphic units.

Depositional Zone 1 (MFA-1 + Unit 1; 1058–966 m)

The different microfacies making up MFA-1 point to deposition taking place in a carbonate ramp setting situated in relatively deep water. The fine-grained limestones of MFA-1 have abrupt erosional contacts with the underlying lithologies and show fine parallel laminations of silt-grade material, which are characteristics of distal turbidites (Stow & Shanmugam, 1980; Piper & Stow, 1991) and indicate that the carbonate deposits were derived from a distal carbonate ramp area. The associated calcareous mudstones and mudstones overlying the limestones represent the topmost layers of a typical calciturbidite succession (Meischner, 1964). In a broader context, the relatively fine-grained Late Viséan limestones of MFA-1 are equivalent to the uppermost part of an overall Dinantian fining-upwards cycle (Mathes-Schmidt, 2000; Van Tongeren & Pagnier, 1987), which further suggests the limestones were deposited in relatively deep water.

The interval from 1058 to 1014 m is composed of strongly silicified limestones, the silica being of biogenic origin from radiolarians and sponge spicules, whereas non-silicified limestones are predominant above 1014 m. The silicified limestones have been assigned to Subunit 1a, which is characterised by higher Si/Zr values than the overlying Subunit 1b, to which the non-silicified limestones have been allocated. Furthermore, the silicified limestones have total organic carbon (TOC) values ranging from 1.33 to 5.48 wt% (Fig. 2), which are the highest TOC values recorded from anywhere over the studied core section and are associated with high U_{org} levels, all of which indicate organic matter to be very common. The abundance of organic carbon is believed to have promoted a synsedimentary, early diagenetic reduction in the pH of the formation waters, with low pH values favouring the solution of carbonate that in turn encouraged silica precipitation (Krauskopf, 1956), which could explain the association between the high TOC values and the profusion biogenic silica (Van Tongeren & Pagnier, 1987).

The mudstones lying between 988 and 991 m are thought to signify the *Actinopteria* Black Shale Event of the Rhenish Mountains and the Harz Mountains (Germany) and correspond to a transgressive systems tract (Herbig, 2011). They are characterised by low Si/Al values, which reflect their increased clay content, whilst their higher Ti, Zr and K levels show they contain more detrital material than the limestones below. The low U_{org} levels recorded from the mudstones show that deposition occurred in oxygenated waters, which are not conducive to the

https://doi.org/10.1017/njg.2015.25 Published online by Cambridge University Press

preservation of organic matter, whereas the reduced log Ca levels point to the drowning of the carbonate platform during the flooding event.

Regression began at the start of Namurian times (Ross & Ross, 1985), resulting in a gradual change in lithology and a shallowing of water depths, with the shallowest water depths in the Namurian being reflected by the presence of the *Girvanella* boundstone found in the uppermost part of MFA-1 – the calcified cyanobacteria *Girvanella* requires shallow water in the photic zone to flourish. The regression is marked within the microfacies association by a reduction in the abundance of lime mudstones and an increase in the abundance of coarser grained wackestones towards the top of MFA-1. In geochemical terms the regression is reflected by upwards increases in the log Ca levels, which signify the relative shallowing of sea level and the concomitant increases in grain size and abundance of calcareous components.

The first recognition of *Planolites* burrows over the core section in the upper part of MFA-1 points to the presence of somewhat variable conditions in the depositional environment (Fig. 3F), as the infauna responsible for this trace fossil required oxygenated bottom waters. This in turn shows that there must have been a transient change in the overall reducing bottom water conditions that prevailed during the time the lithologies making up MFA-1 accumulated, as reflected by high U_{org} levels and the absence of preserved infauna. Furthermore, synaeresis cracks have been noted immediately above the *Planolites*-bearing horizon (Fig. 2). Burst (1965) states that such cracks can be formed by the contraction of clay in response to changes in the salinity of the surrounding liquid, which is a further indication for a change in the overall bottom water conditions.

There is a gradual transition from limestones to calcareous mudstones over the upper part of MFA-1 and thence into the mudstones of MFA-2 belonging to Depositional Zone 2. The transition is accompanied by an upwards decrease in log Ca levels (= decrease in the abundance of calcareous components) and an upwards increase in Al, K and Rb levels (= increase in clay abundance). Such a gradual transition is the result of deposition in an area close to the northern part of the London-Brabant Massif. This area is determined by a synsedimentary block-tectonic and corresponding fluctuating sea levels, especially during the Viséan and Namurian. Hence, abrupt sequence boundaries and unconformities that may have developed in the tectonically more stable parts of the basin are not developed in the studied core section (Mathes-Schmidt, 2000; Kramers et al., 2011).

Depositional Zone 2 (MFA-2 & MFA-3 + Unit 2; 966–917 m)

The microfacies of this zone and the geochemical characteristics of Unit 2 are somewhat variable, which points to fluctuating processes operating in the depositional environment and to detrital material coming from several sources. In addition, the transitional contact of Depositional Zone 2 with Depositional Zone 3 presumably is governed by the palaeogeography.

The successions representing Depositional Zone 2 all belong to the Geverik Member. This assignment contradicts the classical range of this member within the investigated core section from 992 to 926 m (Van Adrichem Boogaert & Kouwe, 1993). According to Van Adrichem Boogaert & Kouwe (1993) it incorporates the first mudstone succession of the investigated core section, i.e. the *Actinopteria* Black Shale Event, which the current study places in Depositional Zone 1. Although this event deposit shows the first significantly higher gamma API values in comparison with the underlying lithologies, it has a different genetic origin compared to the Geverik Member and thus is not part of Depositional Zone 2.

Furthermore, Van Adrichem Boogaert & Kouwe (1993) proposed that the organic lithologies of Depositional Zone 2 are the result of accumulation of fine-grained material in an anoxic basin with restricted circulation, based on the absence of preserved, *in situ* benthic fossils. In contrast, the present authors suggest that sedimentation by erosive bedload was the predominant process operating at the time, along with conditions being temporarily dysoxic, like those responsible for the Toarcian black shales found in the Dutch Central Graben (Trabucho-Alexandre et al., 2012). Consequently, deposition of the Depositional Zone 2 successions probably took place in a distal shelf environment below the storm wave base.

The limestone and mudstone microfacies present over the lower part of Depositional Zone 2 (= MFA-2) are characterised by abundant clay minerals, with sand-grade grains also being relatively common. Unit 2 has lower Si/Al values than Unit 1, coupled with higher Si, Al, K, Rb, Ti and Zr levels. These higher levels show that Depositional Zone 2 contains more detrital material than Depositional Zone 1. Sandy lenticular mudstones are the most frequent lithology encountered over MFA-2, the lenses comprising clay and silt-grade grains being the product of intermittent erosion and bedload transport of mud by relatively strong bottom currents (Schieber et al., 2010). In addition, the contacts between silt-enriched and clay-enriched lenticular laminae are well defined and seem erosional: uninterrupted deposition via settling from suspension would produce diffuse boundaries (Schieber, 1999), a feature not observed over Depositional Zone 2. Furthermore, the seaward transport of detrital sediment from land by bottom currents is consistent with the relatively high content of sand-grade detrital material noted in MFA-2, whereas more finer-grained detrital material would have been expected if deposition occurred by the vertical aggradation of sediment alone.

Some authors have suggested that accumulation of the successions of the Geverik Member, i.e. Depositional Zone 2, have accumulated in anoxic conditions (Van Adrichem Boogaert & Kouwe, 1993). This may have been true for the microfacies

https://doi.org/10.1017/njg.2015.25 Published online by Cambridge University Press

making up MFA-2 (= lower part of Depositional Zone 2), but the predominant fossiliferous mudstones of MFA-3 (= upper part of Depositional Zone 2) were deposited in either permanent dysoxic settings or in environments that were at least temporarily oxygenated. The change from anoxic to dysoxic/temporarily oxygenated depositional environments is reflected by MFA-2 having higher U levels than MFA-3. Under reducing conditions, which typically are brought about by the decay of organic matter, the uranium ions are reduced from U(VI) to U(IV) and the latter are insoluble and therefore accumulate (Lovley et al., 1991). However, uranium is soluble under typical (oxygenated) marine conditions, reflected by its lowered values in MFA-3. Further evidence for oxygenated conditions is also provided by the occurrence of *in situ* benthic fossils in MFA-3. These fossils mostly take the form of monospecific occurrences of trilobites, which could indicate these trilobites were highly specialised benthic organisms adapted to minimum oxygen levels, although bivalves and thin-shelled goniatites are also present. The transport of marine fauna from adjacent shelves and upper-slope settings into an anoxic basin by event deposition, such as slope collapse, as suggested for the Mississippian Barnett Shale (Loucks & Ruppel, 2007), is unlikely. However, other marine organisms, especially soft-bodied varieties, most likely lived on and within the substrate as well, as shown by the presence of disrupted bioclastic laminae. In some cases, these laminae show a downward drag of sediment (Fig. 5B), thus proving disruption occurred prior to any diagenesis or was not the product of tectonism. The characteristic homogeneous fabric of the fossiliferous calcareous mudstones belonging to MFA-3 is believed to be due to bioturbation by epibenthic and endobenthic sea dwellers that colonised the nutrient-rich muddy substrates; predators having larger oxygen requirements due to their high metabolic rates probably were absent (Wignall, 1990).

All the evidence points to the MFA-3 successions being deposited in relatively shallow marine environments, below storm wave base, with minimum oxygen levels. The increase in biogenic activity associated with the MFA-2 to MFA-3 transition could well be reflected by the upwards increase in U_{org} levels across the Subunit 2b–Subunit 2c boundary.

The boundary between MFA-2 and MFA-3 marks the probable environmental change from anoxic conditions to dysoxic conditions brought about by the influx of oxygenated waters, which favoured the colonisation of the substrate by benthic organisms adapted to such conditions. The higher Fe and K levels recorded from MFA-3 reflect the occurrence of more detrital clay, whilst the upward increases in Ti and Rb levels likewise point to greater amounts of detrital material being present, as do low levels of U_{org}. These geochemical characteristics support the premise of oxygenated waters transporting detrital material into the depositional basin and therefore are in accordance with the observed textural features.

Depositional Zone 3 (MFA-4a/4b, MFA-5 & MFA-6 + Unit 3; 917–727 m)

The stratigraphic succession comprising MFA-4a, MFA-5 and MFA-4b is interpreted to reflect repeated deposition in a deltaic setting. Deltaic settings prevailed in the area of deposition during the Namurian (Langenaeker & Dusar, 1992).

The characteristic lenticular fabric of the microfacies making up MFA-4a and MFA-4b was caused by the intermittent erosive bedload transport of soft mud clasts by relatively strong bottom currents (Schieber et al., 2010). Comparable fabrics are reported from other coeval organic strata occurring in the northwestern European Carboniferous Basin (Davies et al., 2012; Könitzer et al., 2014; Nyhuis et al., 2014).

The Namurian successions in northwestern Europe show transgressional–regressional cycles (Ramsbottom, 1977, 1979). The boundaries between the cycles are marked by the occurrence of fauna linked to the transgressional conditions at the start of each cycle (Ramsbottom, 1977). The goniatite-bearing section present within the upper part of MFA-4a, which has been geochemically investigated by Kombrink et al. (2008b), is regarded as defining the start of such a transgressional cycle. On a broader scale, the funnel-shaped gamma-ray motifs associated with the coarsening-upwards Namurian successions penetrated by the study well possibly reflect repeated delta progradation into a predominantly lacustrine basin (see Van Adrichem Boogaert & Kouwe (1993) and references therein).

However, it has to be noted that delta progradation into a predominantly lacustrine basin may well apply to the coal-bearing Upper Namurian successions (Van Tongeren & Pagnier, 1987), but not to the lower Namurian strata assigned to Depositional Zone 3 (= Epen Formation). Although high Ti, Fe, K and Zr levels show detrital material is common in this zone, the general absence of a fully marine fauna, e.g. goniatites, does not necessarily support the statement that deposition took place in a non-marine environment since goniatites are highly facies dependent. Slight changes in the environmental conditions, such as the observed increased terrigeneous input, could therefore have caused a marine accumulation devoid of goniatites within this zone. In addition, extensive bedload transport and high sedimentation rates have favoured reworking of shell material, which may be another explanation for this feature.

The bioturbated to laminated silty mudstones that are predominant in MFA-5 are the products of cyclic deposition followed by erosion, redeposition and bioturbation, with the simple feeding structures such as *Planolites* and *Teichichnus* being noted, which are common trace fossils in mudstones (Wetzel & Uchmann, 1998). The degree of bioturbation largely depends on the numbers of infaunal organisms relative to the rate of deposition (Blatt, 1992). For instance, rates of deposition would be high in the proposed prodelta environment, resulting in burrows being rapidly extended to keep pace with deposition, as has been shown for *Teichichnus* (MacEachern et al., 2009;

https://doi.org/10.1017/njg.2015.25 Published online by Cambridge University Press

see also Fig. 7A), the presence of which indicates high-energy depositional environments (Hovikoski et al., 2008; MacEachern et al., 2009). *Teichichnus* belongs to the *Cruziana* ichnofacies of Seilacher (1967): the ichnofacies is indicative of mid and distal marine settings below normal wave base, so the occurrence of *Teichichnus* conforms with the proposed depositional environment for MFA-5. The other observed burrows, e.g. *Planolites* (Fig. 7B), presumably were adjusted when depositional rates slowed, which in turn points to the cyclic nature of deposition.

The fact that ichnofossils are restricted to MFA-5 shows that oxygen levels conducive to infaunal colonisation of the substrate must have existed for some time at least. The organism responsible for constructing *Planolites* burrows presumably extracted oxygen from the sediment pore waters, so its presence therefore proves the occurrence of oxygenated sediments in shallower tiers (Rodríguez-Tovar & Uchman, 2010). In summary, the microfacies making up MFA-5 indicate variable, but relatively high, rates of deposition operated in an overall oxygenated environment suitable for benthic organisms, whereas the microfacies belonging to Depositional Zone 3, i.e. MFA-4a and MFA-4b, reflect relatively constant rates of deposition in anoxic settings that together hampered significant infaunal activity.

The cross-stratified and locally bioturbated siltstones and sandstones of MFA-6 reflect deposition in proximal marine settings where detrital material was readily available.

To conclude, the observed features of the successions allocated to Depositional Zone 3 point to deposition in a marine prodelta slope environment.

Conclusions

Detailed microfacies analysis has been undertaken on a 332-m thick core section from the southern Netherlands covering upper Mississippian successions. The results of this analysis have added to the current knowledge regarding the different genetic aspects and microfacies variability relating to the fine-grained, organic-rich Carboniferous strata in this area. Variations in the geochemistry of successions as determined by pXRF analyses provided corroborative information for the environmental interpretation and contributed to a clearer understanding of the complex interplay between changes in the microfacies and the interpreted mineralogy of the strata in question.

Six microfacies associations (MFA-1 to MFA-6), three chemostratigraphic units (Unit 1 to Unit 3) and 13 chemostratigraphic subunits have been identified over the core section. Integrated interpretations of microfacies associations and chemostratigraphic zonation led to the recognition of Depositional Zones 1 to 3, which in turn show how depositional environments changed during time.

During Late Viséan times, fine-grained turbiditic limestones were emplaced in a distal carbonate ramp setting, whereas at the end of the Viséan/start of the Namurian these turbiditic limestones became intercalated with mudstones having some similarities to the *Actinopteria* Black Shale Event that has been documented in the Rhenish Mountains and the Harz Mountains in Germany. This event is isochronous and its recognition would thus aid interwell correlations. The lithologically transitional part of the lowermost Namurian consists of successions comprising heterogeneous lithologies, although mudstones are predominant. These successions belong to the Geverik Member and have been assigned to Depositional Zone 2 (= MFA-2 & MFA-3 + Unit 2). Previously, the member was thought to correspond to the core interval between 992 and 926 m over the core section. Based on evidence provided by this study the Geverik Member has been reassigned to the interval between 966 and 917 m. Moreover, Depositional Zone 2 (i.e. the Geverik Member) successions were deposited during a period of fluctuating sea levels and they show the first evidence in the core section for increased infaunal activity and sedimentation by erosive bedload transport. This contradicts previously held views that deposition occurred in anoxic settings and sedimentation was predominantly by vertical aggradation. Deltaic environments developed later on in the Namurian show that high depositional rates and benthic colonisation of the substrate was temporarily favoured.

Acknowledgements

C. Nyhuis acknowledges Wintershall Holding GmbH, especially S. Aarburg, for providing a unique forum of interdisciplinary scientific work and financial support. A fellowship grant to C. Nyhuis from the Graduate School of Geosciences (GSGS) University of Cologne is gratefully acknowledged. Moreover, we are grateful to D. Korn for his valuable comments on biostratigraphy. M. Mathes-Schmidt is thanked for access to important thin sections. Prof. H.-G. Herbig, D. Wright and T. Pearce are acknowledged for reviewing earlier versions of the manuscript. We also thank J.W. Weegink, A. Klomp and R. de Wilde for dedicated support at TNO's core storage. Finally, we thank an anonymous reviewer, H. Kombrink, and H. Verweij for constructive and supportive comments.

References

Abouelresh, M.O. & ***Slatt, R.M.***, 2012. Lithofacies and sequence stratigraphy of the Barnett Shale in east-central Fort Worth Basin, Texas. AAPG Bulletin 96: 1–22.

Amler, M., 2006. Bivalven und Rostroconchien. In: Amler, M.R.W. & Stoppel, D. (eds): Stratigraphie von Deutschland VI, Unterkarbon (Mississippium). Schriftenreihe der Deutschen Gesellschaft für Geowissenschaften 41: 121–146.

https://doi.org/10.1017/njg.2015.25 Published online by Cambridge University Press

Blatt, H., 1992. Sedimentary Petrology. Freeman and Co. (New York): 514 pp.

Burst, J.F., 1965. Subaqueously formed shrinkage cracks in clay. Journal of Sedimentary Research 35: 348–353.

Caplan, M.L. & ***Bustin, R.M.***, 2001. Palaeoenvironmental and palaeoceanographic controls on black, laminated mudrock deposition: example from Devonian–Carboniferous strata, Alberta, Canada. Sedimentary Geology 145: 45–72.

Davies, S.J., ***Leng, M.J.***, ***Macquaker, J.H.S.*** & ***Hawkins, K.***, 2012. Sedimentary process control on carbon isotope composition of sedimentary organic matter in an ancient shallow-water shelf succession. Geochemistry, Geophysics, Geosystems 13: 1525–2027.

Davydov, V.I., ***Korn, D.*** & ***Schmitz, M.D.***, 2012. The Carboniferous Period. In: ***Gradstein, F.***, ***Ogg, J.***, ***Schmitz, M.*** & ***Ogg, G.*** (eds): The Geological Time Scale. Elsevier (Amsterdam): 603–651.

Dunham, R.J., 1962. Classification of carbonate rocks according to depositional texture. In: ***Ham, W.E.*** (ed.): Classification of carbonate rocks: American Association of Petroleum Geologists Memoir: 108–121.

Gerling, P., ***Geluk, M.C.***, ***Kockel, F.***, ***Lokhorst, A.***, ***Lott, G.K.*** & ***Nicholson, R.A.***, 1999. 'NW European Gas Atlas' – New implications for the Carboniferous gas plays in the western part of the Southern Permian Basin. In: Fleet, A.J. & Boldy, S.A.R. (eds): Petroleum Geology of Northwest Europe: Proceedings of the 5th Conference. Geological Society (London): 799–808.

Hartwig, A., ***Könitzer, S.***, ***Boucsein, B.***, ***Horsfield, B.*** & ***Schulz, H.-M.***, 2010. Applying classical shale gas evaluation concepts to Germany – Part II: Carboniferous in Northeast Germany. Chemie der Erde 70: 93–106.

Herbig, H.-G., 2011. Stratigraphische Sequenzen und Bioevents im Kulmbecken des Rheinischen Schiefergebirges (Mississippium, Deutschland). In: Ehrmann, W. & Röhling, H.-G. (eds): 100 Jahre Hermann Credner-Stiftung der Deutschen Gesellschaft für Geowissenschaften (Beiträge des Festkolloquiums am 4. und 5. November in Leipzig). Schriftenreihe der Deutschen Gesellschaft für Geowissenschaften 77: 37–39.

Hovikoski, J., ***Lemiski, R.***, ***Gingras, M.***, ***Pemberton, G.*** & ***MacEachern, J.A.***, 2008. Ichnology and sedimentology of a mud-dominated deltaic coast: Upper Cretaceous Alderson Member (Lea Park Fm), Western Canada. Journal of Sedimentary Research 78: 803–824.

Kerschke, D. & ***Schulz, H.-M.***, 2013. The shale gas potential of Tournaisian, Visean, and Namurian black shales in North Germany: baseline parameters in a geological context. Environmental Earth Sciences 70: 3817–3837.

Kombrink, H., ***Leever, K.A.***, ***Van Wees, J.-D.***, ***Van Bergen, F.***, ***David, P.*** & ***Wong, T.E.***, 2008a. Late Carboniferous foreland basin formation and Early Carboniferous stretching in northwestern Europe: inferences from quantitative subsidence analyses in the Netherlands. Basin Research 20: 377–395.

Kombrink, H., ***van Os, B.J.H.***, ***van der Zwan, C.J.*** & ***Wong, T. E.***, 2008b. Geochemistry of marine and lacustrine bands in the Upper Carboniferous of the Netherlands. Netherlands Journal of Geosciences—Geologie en Mijnbouw 87: 300–322.

Kombrink, H., ***Besly, B.M.***, ***Collinson, J.D.***, ***Den Hartog Jager, D.G.***, ***Drozdzewski, G.***, ***Dusar, M.***, ***Hoth, P.***, ***Pagnier, H.J.M.***, ***Stemmerik, L.***, ***Waksmundzka, M.I.*** & ***Wrede, V.***, 2010. Carboniferous. In: Doornenbal, J.C. & Stevenson, A.G. (eds): Petroleum Geological Atlas of the Southern Permian Basin Area. EAGE Publications b.v. (Houten): 81–99.

Könitzer, S.F., ***Davies, S.J.***, ***Stephenson, M.H.*** & ***Leng, M.J.***, 2014. Depositional controls on mudstone lithofacies in a basinal setting: Implications for the delivery of sedimentary organic matter. Journal of Sedimentary Research 84: 198–214.

Korn, D., 2008. Early Carboniferous (Mississippian) calciturbidites in the northern Rhenish Mountains (Germany). Geological Journal 43: 151–173.

Kraft, T., 1992. Faziesentwicklung vom Flözleeren zum Flözführenden Oberkarbon (Namur B-C) im südlichen Ruhrgebiet. PhD thesis, Ruhr-Universität Bochum: 255 pp.

Kramers, L., ***van Wees, J.-D.***, ***Wassing, B.***, ***Kronimus, A.***, ***Urai, J.L.***, ***Kukla, P.A.*** & ***Bekendam, R.***, 2011. Studie naar Haalbaarheid van OPAC op de locatie Graetheide en nabije omgeving. rapport nr. TNO-060-UT-2011–01251 (Utrecht).

Krauskopf, K.B., 1956. Dissolution and precipitation of silica at low temperatures. Geochimica et Cosmochimica Acta 10: 1–26.

Langenaeker, V. & ***Dusar, M.***, 1992. Subsurface facies analysis of the Namurian and earliest Westphalian in the western part of the campine Basin (N Belgium). Geologie en Mijnbouw 71: 161–172.

Lemiski, R.T., ***Hovikoski, D.J.***, ***Pemberton, D.S.G.*** & ***Gingras, D. M.***, 2011. Sedimentological ichnological and reservoir characteristics of the low-permeability, gas-charged Alderson Member (Hatton gas field, southwest Saskatchewan): Implications for resource development. Bulletin of Canadian Petroleum Geology 59: 27–53.

Littke, R., ***Krooss, B.***, ***Uffmann, A.K.***, ***Schulz, H.-M.*** & ***Horsfield, B.***, 2011. Unconventional gas resources in the Paleozoic of Central Europe. Oil and Gas Science Technology – Review IFP Energies Nouvelles 66: 953–977.

Loucks, R.G. & ***Ruppel, S.C.***, 2007. Mississippian Barnett Shale: Lithofacies and depositional setting of a deep-watershale-gas succession in the Fort Worth Basin, Texas. AAPG Bulletin 4: 579–601.

Lovley, D.R., ***Phillips, E.J.P.***, ***Gorby, Y.A.*** & ***Landa, E.R.***, 1991. Microbial reduction of uranium. Nature 350: 413–416.

MacEachern, J.A., ***Pemberton, S.G.***, ***Bann, K.L.*** & ***Gingras, M.K.***, 2009. Departures from the archetypal ichnofacies: Effective recognition of physiochemical stresses in the rock record. In: MacEachern, J.A., Bann, K.L., Gingras, M.K. & Pemberton, S.G. (eds): Applied Ichnology. SEPM Short Course Notes 52: 65–94.

Mathes-Schmidt, M.E., 2000. Mikrofazies, Sedimentationsgeschehen und paläogeographische Entwicklung im Verlauf des oberen Viséums im Untergrund der Niederrheinischen Bucht und des Campine-Beckens. PhD thesis. Rheinisch-Westfälisch Technische Hochschule (Aachen): 245 pp.

Meischner, K.D., 1964. Allodapische Kalke, Turbidite in Riff-Nahen Sedimentations-Becken. In: Bouma, A.H. & Brouwer, A. (eds): Developments in Sedimentology. Elsevier (Amsterdam): 156–191.

Nyhuis, C.J., ***Rippen, D.*** & ***Denayer, J.***, 2014. Facies characterization of organic-rich mudstones from the Chokier Formation (lower Namurian), south Belgium. Geologica Belgica 17: 311–322.

Nyhuis, C.J., ***Amler, M.R.W.*** & ***Herbig, H.-G.***, 2015. Facies and palaeoecology of the late Viséan (Mississippian) *Actinopteria* Black Shale Event in the Rhenish Mountains (Germany). Zeitschrift der Deutschen Gesellschaft für Geowissenschaften 166: 55–69.

Pearce, T.J., ***Wray, D.S.***, ***Ratcliffe, K.T.***, ***Wright, D.K.*** & ***Moscariello, A.***, 2005. Chemostratigraphy of the Upper Carboniferous Schooner Formation, southern North Sea. In: Collinson, J.D., Evans, D.J., Holliday, D.W. & Jones, N.S. (eds): Carboniferous hydrocarbon geology: the southern North Sea and surrounding

https://doi.org/10.1017/njg.2015.25 Published online by Cambridge University Press

onshore areas. Yorkshire Geological Society, Occasional Publications Series 7: 147–163.

Piper, D.J.W. & ***Stow, D.A.V.***, 1991. Fine-grained turbidites. In: Einsele, G., Ricken, W. & Seilacher, A. (eds): Cycles and Events in Stratigraphy. Springer (Heidelberg): 361–376.

Potts, P.J. & ***Kane, J.S.***, 2003. International association of Geoanalysis Certificate of Analysis: Certified Reference Material OU-6 (Penrhyn Slate). Geostandards and Geoanalytical Research 29: 233–236.

Ramsbottom, W.H.C., 1977. Major cycles of transgression and regression (mesothems) in the Namurian. Proceedings of the Yorkshire Geological Society 41: 261–291.

Ramsbottom, W.H.C., 1979. Rates of transgression and regression in the Carboniferous of NW Europe. Journal of the Geological Society 136: 147–153.

Ratcliffe, K.T. & ***Wright, A.M.***, 2012. Unconventional methods for unconventional plays:using elemental data to understand shale resource plays Part 1. PESA News Resources April/May 2012: 89–93.

Ratcliffe, K.T., ***Wright, A. M.***, ***Montgomery, P.***, ***Palfrey, A.***, ***Vonk, A.***, ***Vermeulen, J.*** & ***Barrett, M.***, 2010. Application of chemostratigraphy to the Mungaroo Formation, the Gorgon Field, offshore Northwest Australia. Australian Petroleum Production and Exploration Association Journal 50: 371–385.

Ratcliffe, K.T., ***Woods, J.*** & ***Rice, C.***, 2012a. Determining well-bore pathways during multilateral drilling campaigns in shale resource plays: an example using chemostratigraphy from the Horn River Formation, British Columbia, Canada. Eastern Australasian Basins Symposium IV: 143–148.

Ratcliffe, K.T., ***Wright, A.M.*** & ***Schmidt, K.***, 2012b. Application of inorganic whole-rock geochemistry to shale resource plays: an example from the Eagle Ford Shale Formation, Texas. The Sedimentary Record 10: 4–9.

Reed, F.S. & ***Mergner, J.L.***, 1953. Preparation of rock thin sections. American Mineralogist 38: 1184–1203.

Rodríguez-Tovar, F.J. & ***Uchman, A.***, 2010. Ichnofabric evidence for the lack of bottom anoxia during the lower Toarcian. Oceanic Anoxic Event in the Fuente de la Vidriera section, Betic Cordillera, Spain. Palaios 25: 576–587.

Röhl, H.-J., ***Schmid-Röhl, A.***, ***Oschmann, W.***, ***Frimmel, A.*** & ***Schwark, L.***, 2001. The Posidonia Shale (Lower Toarcian) of SW-Germany: an oxygen-depleted ecosystem controlled by sea level and palaeoclimate. Palaeogeography, Palaeoclimatology, Palaeoecology 165: 27–52.

Ross, C.A. & ***Ross, J.R.P.***, 1985. Late Paleozoic depositional sequences are synchronous and worldwide. Geology 13: 194–197.

Rowe, H., ***Ruppel, S.***, ***Rimmer, S.*** & ***Loucks, R.***, 2009. Core-based chemostratigraphy of the Barnett Shale, Permian Basin, Texas. Gulf Coast Association of Geological Societies Transactions 59: 675–686.

Rowe, H., ***Hughes, N.*** & ***Robinson, K.***, 2012. The quantification and application of handheld energy-dispersive x-ray fluorescence (ED-XRF) in mudrock chemostratigraphy and geochemistry. Chemical Geology 324–325: 122–131.

Ruprecht, L., 1937. Die Biostratigraphie des obersten Kulm im Sauerlande. Jahrbuch der Preußischen Geologischen Landesanstalt (für 1936) 57: 238–283.

Schieber, J., 1989. Facies and origin of shales from the Mid-Proterozoic Newland Formation, Belt Basin, Montana, USA. Sedimentology 36: 203–219.

Schieber, J., 1999. Distribution and deposition of mudstone facies in the Upper Devonian Sonyea Group of New York. Journal of Sedimentary Research 69: 909–925.

Schieber, J., ***Southard, J.B.*** & ***Schimmelmann, A.***, 2010. Lenticular shale fabrics resulting from intermittent erosion of muddy sediments–Comparing observations from flume experiments to the rock record. Journal of Sedimentary Research 80: 119–128.

Seilacher, A., 1967. Biogenic sedimentary structures. In: Imbrie, J. & Newell, N. (eds): Approaches to Paleoecology. Wiley (New York): 296–316.

Stow, D.A.V. & ***Shanmugam, G.***, 1980. Sequence of structures in fine-grained turbidites: Comparison of recent deep-sea and ancient flysch sediments. Sedimentary Geology 25: 23–42.

Svendsen, J., ***Friis, H.***, ***Stollhofen, H.*** & ***Hartley, N.***, 2007. Facies discrimination in a mixed fluvio-eolian setting using elemental whole-rock geochemistry–Applications for reservoir characterization. Journal of Sedimentary Research 77: 23–33.

Trabucho-Alexandre, J., ***Dirkx, R.***, ***Veld, H.***, ***Klaver, G.*** & ***de Boer, P.L.***, 2012. Toarcian black shales in the Dutch Central Graben: Record of energetic, variable depositional conditions during an oceanic anoxic event. Journal of Sedimentary Research 82: 104–120.

Tribovillard, N., ***Algeo, T.J.***, ***Lyons, T.*** & ***Riboulleau, A.***, 2006. Trace metals as paleoredox and paleoproductivity proxies: An update. Chemical Geology 232: 12–32.

Uffmann, A.K., ***Littke, R.*** & ***Rippen, D.***, 2012. Mineralogy and geochemistry of Mississippian and Lower Pennsylvanian Black Shales at the Northern Margin of the Variscan Mountain Belt (Germany and Belgium). International Journal of Coal Geology 103: 92–108.

Van Adrichem Boogaert, H.A. & ***Kouwe, W.F.P.***, 1993. Stratigraphic nomenclature of the Netherlands, revision and update by RGD and NOGEPA. Mededelingen Rijks Geologische Dienst 50: 1–40.

Van Amerom, H.W.J., 1986. Cumulatief rapport betreffende de stratigrafie van de boring Geverik. Internal report 2132. Rijks Geologische Dienst (Heerlen).

Van Bergen, F., 2011. Evaluation of the potential of shale gas in the Netherlands. Geophysical Research Abstracts 13: EGU 2011–7793–2011.

Van Tongeren, P.C.H. & ***Pagnier, H.J.M.***, 1987. Onderzoeksresultaten van boring Geverik-1 (OPAC-studie Zuid-Limburg). Internal report 2144. Rijks Geologische Dienst (Heerlen).

Wetzel, A. & ***Uchmann, A.***, 1998. Biogenic sedimentary structures in mudstones – an overview. In: Schieber, J., Zimmerle, W. & Sethi, P. (eds): Shales and Mudstones, Vol. 1. Schweizerbart (Stuttgart): 351–369.

Wignall, P.B., 1990. Observations on the evolution and classification of dysaerobic communities. In: Miller III, W. (ed.): Paleocommunity temporal dynamics: The long-term development of multispecies assemblies. Paleontological Society Special Publications 5: 99–111.

https://doi.org/10.1017/njg.2015.25 Published online by Cambridge University Press